FIRST SYSTEM-LEVEL DEMONSTRATION OF HIGH-CONTRAST FOR FUTURE SEGMENTED SPACE TELESCOPES

R. Soummer, M. Perrin and the HiCAT team:

Co-Investigators: G. Brady, K. Brooks, T. Comeau, J. Fowler, R. Gontrum, H. Kuntz, I. Laginja, C. Moriarty, J. Noss, P. Petrone, L. Pueyo, A. Sivaramakrishnan, K. St.Laurent, J. Tumlinson, N. Scott, S. Will
Collaborators: S. Bailey, A. Brito, M. Ferrari, T. Fusco, T. Groff, J. Hagopian, R. Juanola-Parramon, L. Leboulleux, L. Mugnier, J. Mazoyer, M. N'Diaye, E. Por, A.J. Eldorado Riggs, J.F. Sauvage, C. Stark, N. Zimmerman
Undergraduate students: E. McChesney, A. Doran, M. Grenville, N. Lamaison, S. Pourshalchi, S. Rajpurohit, L. Reider, T. Tiberghien-Alvarez,

May 2019

Approvals

Released by:

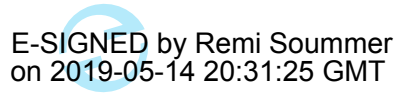

Remi Soummer — Date
Principal Investigator, STScI

Approved by:

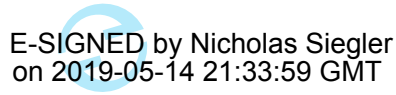

Nicholas Siegler — Date
Exoplanet Exploration Program Chief Technologist, NASA JPL

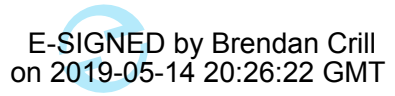

Brendan Crill — Date
Exoplanet Exploration Program Deputy Chief Technologist, NASA JPL

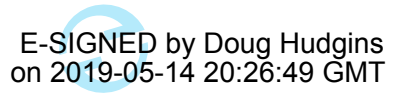

Douglas Hudgins — Date
Exoplanet Exploration Program Scientist, NASA HQ

CONTENTS

1. OBJECTIVE

The objective of this three-year program is to advance high-performance coronagraph systems technology readiness levels (TRL) for terrestrial planet direct imaging missions of the future with segmented aperture space telescopes. The work will be conducted on our High-contrast Imager for Complex Aperture Telescopes (HiCAT) experiment which uses the Apodized Pupil Lyot Coronagraph (APLC) approach to segmented apertures. By optimizing individual components, we have already matured the technology to TRL 3. But for a segmented telescope aiming to achieve 10^{-10} starlight suppression, the stability of the wavefront delivered from the telescope presents special challenges to coronagraph performance. The telescope and coronagraph must be considered together and their technologies advanced as an integrated system.

This objective of this program is thus to take the next logical step in segmented coronagraph technology, achieving TRL 4 first at the component level, then TRL 4 in a full-system context. Our roadmap to raise the system-level TRL for high-contrast coronagraphy on segmented apertures will require the following major technical tasks:

1. Ongoing advancement of the shaped-pupil APLC as an individual component, including refinements to mask designs, hardware optimization and tolerancing, and understanding of the impacts of segment-level aberrations.
2. Advancing the readiness of the integrated system, with the coronagraph and a multi-layered wavefront control system working together to sense and correct for dynamic instabilities on the spatial and temporal frequencies of interest in a segmented observatory.
3. Refining and validating performance models for segmented coronagraphy over a range of spatial and time scales, both to directly support the prior two tasks, and to provide improved modeling capabilities for future vacuum tests and mission design studies.

2. INTRODUCTION AND BACKGROUND

2.1. **Methods for High-Contrast Exoplanet Imaging.** The discovery and study of worlds that could potentially support life has emerged as perhaps the most compelling science driver for future large space observatories. A "New Worlds Mission" that obtains direct spectroscopic measurements of terrestrial planet atmospheres would enable us to search for signatures of habitability and seek out potential molecular markers of distant biologies. Indeed, three of the four large mission concept studies for the 2020 decadal survey have exoplanets as a central driving science goal: the Large Ultraviolet, Optical and InfraRed observatory (LUVOIR), the Habitable Exoplanet Observatory (HabEx), and the Origins Space Telescope (OST). The spectroscopic characterization of terrestrial exoplanets is both scientifically profound and potentially transformative for humanity's understanding of our place in the cosmos, and is also a topic of tremendous public interest within the US and worldwide.

An observatory's capability for imaging rocky exoplanets turns out to be a steep function of primary mirror diameter, driving us toward the largest possible apertures [Stark et al., 2014, 2015]. Building on the James Webb Space Telescope's (JWST) technologies, segmented mirror architectures can break through the hard limits that launch vehicle fairings place on the sizes of monolithic mirrors [Feinberg et al., 2014]. LUVOIR has baselined a 15-m telescope, with a 9-m alternate, both segmented, and the latter possibly off-axis. HabEx is studying a 6.5 m segmented telescope as its alternative to its 4 m monolith primary architecture. When calculating exo-Earth "yields", or the number of rocky planets in the habitable zone that a mission can detect in a fixed time, these studies usually assume nominal starlight suppression to 10^{-10}, which translates into yields of a

few to a few dozen exo-Earth candidates for apertures of $4-15$ m. Achieving coronagraphy at this demanding level of performance on a large segmented aperture will enable discovery of dozens of terrestrial planets and robust atmospheric characterizations in only a few years of total mission time.

Starlight suppression systems have made substantial progress in the past few years, especially with the Wide Field InfraRed Space Telescope CoronaGraphic Instrument (WFIRST CGI) technology program reaching Technology Readiness Level (TRL) 5 for the coronagraph. [Poberezhskiy et al., 2014, Goullioud et al., 2014, Krist et al., 2016, Cady et al., 2017, 2016, Seo et al., 2017, 2016, Shi et al., 2017]. The further development and flight of CGI would raise these key technologies to TRL 9, and could begin the possible characterization of Jovian planets in reflected light — thereby playing an essential role in preparing for a "search for life" flagship mission. WFIRST's 2.4 m primary remains too small for a "search for life" mission and will not address the technical challenges that are specific to segmented apertures. Yet, segmented architectures also bring new challenges at both the component and system levels. Coronagraph masks must be carefully optimized for segmented pupils. Segment control must be integrated to mitigate drifts along with the high contrast wavefront control and line-of-sight pointing control systems, leading to a web of interconnected control loops communicating on different timescales. A complex trade space exists between the performance of individual subsystems, for instance trading between passive stability and active control, or between coronagraph throughput, inner working angle, and sensitivity to misalignments. Addressing these challenges is the central theme of this program.

2.2. **Description of HiCAT.** Our HiCAT testbed (High contrast imager for Complex Aperture Telescopes, N'Diaye et al., 2013a, 2014a, 2015, Leboulleux et al., 2016, 2017, Moriarty et al., 2018, Soummer et al., 2018)) is currently operational and entirely dedicated to a LUVOIR-type coronagraphic demonstration. It offers an ideal platform for system-level experiments in ambient conditions in the next few years, to pave the way for higher TRL demonstrations in vacuum. This development plan, directly parallel to the WFIRST CGI staged ambient and vacuum experiments, will mature these key technologies needed for future NASA observatories of unprecedented size.

The HiCAT testbed incorporates three deformable mirrors (DMs): two Boston Micromachines 952-actuator micro electro mechanical (MEMS) "kilo-DMs" and an Iris AO 37-element hexagonally-segmented DM. The testbed also includes a fast tip tilt system and extensive supporting metrology suite (custom interferometric metrology for critical hardware elements, phase retrieval channel, theodolites, cameras). An overview of the laboratory facilities is provided in Figure 1. The Apodized Pupil Lyot Coronagraph includes apodizers manufactured using carbon nanotubes grown on a customized catalyst for the black areas, and protected silver or gold for the reflective areas (see Figure 2). As part of this program, we will also compare these apodizers with other manufacturing techniques, such as the silicon grass developed and used at the Jet Propulsion Laboratory (JPL) for WFIRST-CGI [Balasubramanian et al., 2017]. HiCAT has demonstrated the first high-contrast dark zone with a segmented aperture coronagraph operating on an actual segmented pupil, achieving initial contrasts of 1.7×10^{-6} monochromatic and 6.3×10^{-6} in 6% broadband with our latest APLC design operating in air (see Figure 3). This result, combined with numerical modeling of segmented aperture coronagraphy established TRL 3 for a segmented aperture coronagraph (analytical and experimental critical function and/or characteristic proof-of-concept) prior to the starting point of this TDEM program.

FIGURE 1. Russell B. Makidon Optics Laboratory Facilities and Equipment. Cleanroom facilities provide cleanliness (operated at ISO-6 / class 1000 level), temperature and humidity controlled environment. Cleanroom #1 hosts the JWST Optical Simulation Testbed (JOST). Cleanroom #2 and #3 host the *HiCAT testbed* and its associated *Metrology Testbed* described in this proposal. General major equipment includes several light sources (laser diodes, HeNe laser, supercontinuum laser and tunable filter). The metrology testbed includes a Fizeau interferometer, and the lab can borrow a coordinate measurement machine and Theodolites when needed. The HiCAT testbed includes three deformable mirrors, several cameras, and piezo tip/tilt control.

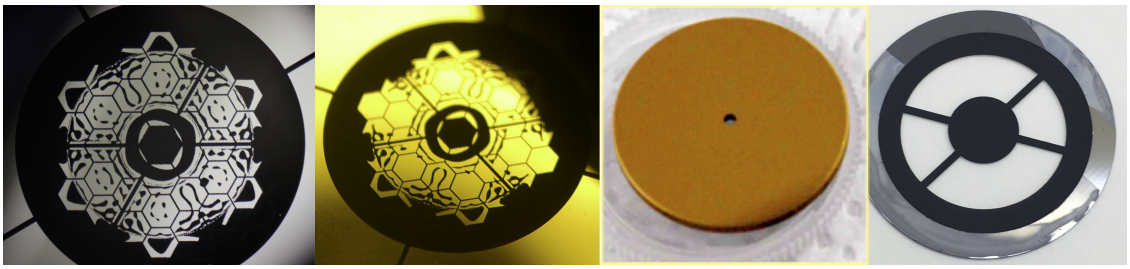

FIGURE 2. *Left 2 panels:* First carbon nanotubes apodizers (manufactured by Advanced Nanophotonics Inc. Hagopian et al., 2010) for an on-axis segmented aperture, on silver and gold. The hemispherical reflectance of carbon nanotubes on these apodizers is 0.5%. Our next batch will target reflectance below 0.1%, comparable or better than JPL's silicon grass used for the WFIRST CGI masks [Balasubramanian et al., 2017]. In theory, carbon nanotubes can reach hemispherical reflectance down to about 0.05%. They offer potentially better surface figure because they involve growth on a catalyst instead of surface etching. While still a research topic, catalyst customization could be used to enable non binary masks with gray areas. There are no limitations for the reflective surface (e.g. silver and gold, as shown here). Note the slightly different patterns with some fully reflective segments in the gold case. Recent wavefront control algorithms (e.g. Adaptive Compensation of Aperture Discontinuities - Optimized Stroke Minimization (ACAD-OSM); Mazoyer et al., 2018a,b) will be tested on this "modified" apodizer pattern. *Panel 3:* Reflective focal plane mask allows natural implementation of Low-Order WaveFront Sensor (LOWFS); mask re-used from former "Lyot Project" courtesy R. Oppenheimer, American Museum of Natural History. *Panel 4:* Corresponding Lyot Stop with x-shaped support structures, also coated with carbon nanotubes on a through-etched silicon wafer. Our latest (early 2019) carbon nanotubes apodizer reached 0.25% hemispherical reflection at the HiCAT wavelengths (around HeNe). The coatings can in theory reach 0.05% [Hagopian et al., 2010] and our goal for HiCAT is to reach 0.1%, comparable or better to the black-Si grass developed at JPL for WFIRST-CGI, which reached 0.15% and has demonstrated contrast close to 10^{-9} [Balasubramanian et al., 2017]; The WFIRST-CGI demonstrated results are about one order of magnitude better than the HiCAT goals. In addition, we have plans to test the JPL silicon-grass on HiCAT during this TDEM. Therefore, we consider apodizer coating capabilities to be low risk for achieving our contrast goals.

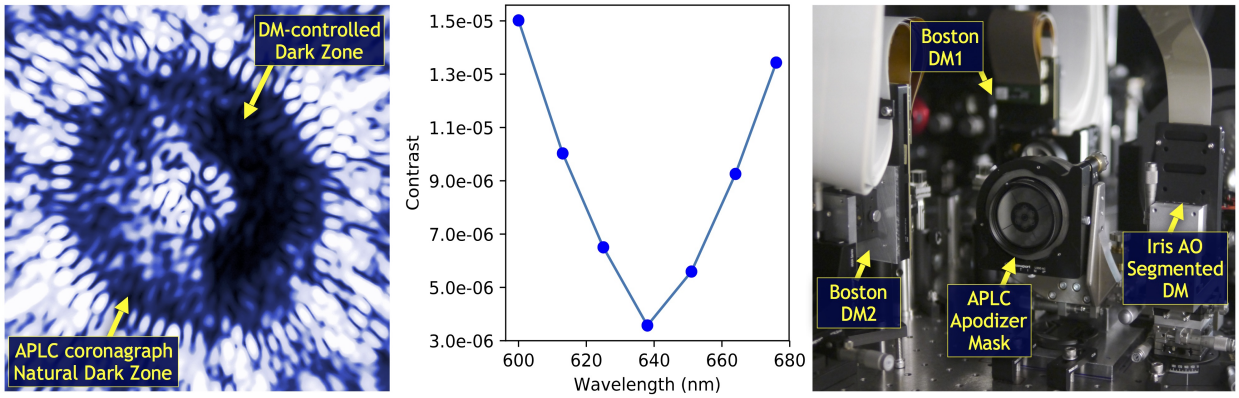

FIGURE 3. *Left:* First demonstration of a coronagraph dark zone with a segmented aperture on-axis telescope simulator (monochromatic contrast: 1.7×10^{-6}, broadband contrast 6.3×10^{-6} in 6% bandpass — average contrast over the entire dark zone, calculated over a photometric aperture). Note the "natural" circular dark zone of the APLC, and the deeper dark zone on the right from wavefront control. *Center:* Broadband demo using a tunable laser (not yet fully optimized in this experiment, with minimum contrast about 2x higher than our best monochromatic result). *Right:* HiCAT testbed with three DMs and carbon nanotube APLC apodizer. ***Note:*** *These results were obtained upon installation of the segmented DM and controlling just one continuous DM (others set to flat); it does not represent the limits of the testbed.*

3. MILESTONE DEFINITIONS

3.1. **TRL 4 component demo of APLC on segmented aperture (Milestone #1).** *Demonstrate $\sim 10^{-7}$ contrast with an APLC on a static segmented aperture in 360 degree dark hole extending from ~ 4.5 to 12 λ/D, in a 6% band centered at 638 nm. The milestone will include a comparison demonstrating agreement between experimental data and analytical or end-to-end numerical modeling.* See Definitions section §5.1 for the precise details of how we intend to measure contrast and other parameters.

Our first milestone extends our past results to a higher contrast (goal: 10^{-7} contrast, i.e. $\geq 10\times$ improvement), through two-DM broadband control to produce $\sim 360^{\circ}$ dark zones in "static" experiments (i.e. without introducing time-variable drifts; the system will be slightly dynamic based on the environment). The segmented DM will be commanded to a flat setting for this demonstration. The main tasks towards this milestone will include:

- Implementation of 2DM control using existing algorithms, with demonstrated operation on a segmented aperture and APLC.
- Expanding our modeling efforts, both analytically (Pair-based Analytical model for Segmented Telescopes Imaging from Space; PASTIS) and numerically, to produce medium-fidelity end-to-end simulations and preliminary error budgeting to explain performance behavior [Leboulleux et al., 2018].
- New apodizer manufacturing for incremental design improvements, incorporating theoretical improvements in the solutions from Segmented-aperture Coronagraph Design and Analysis (SCDA) study [St. Laurent et al., 2018], apodizer coating optimization;
- Experimental validation of APLC robustness to controlled jitter and drifts produced by the piezo tip-tilt stage, and to Lyot stop misalignments.

This task will be supported by hardware and/or alignment enhancements as needed to gain in stability and performance, based on performance limiting factors identified through experiments and modeling. These enhancements or upgrades will be the focus toward the end of Year 1, preceding the milestone demonstration by 2019-12-13, and will likely extend into the beginning of Year 2.

The demonstration of agreement between test data and theoretical predictions will include a range of analyses, such as comparison of data with end-to-end modeling, and analytical error budgeting to estimate limiting contributions to the full system contrast performance (detector noise, DM quantization, mechanical stability, air turbulence, alignment accuracy, mask tolerances, optics quality, etc.)

3.2. **TRL 4 system-level static demo (Milestone #2a).** *Demonstrate closed-loop high-contrast wavefront control in the presence of static segment misalignments, in particular by the operation of a LOWFS to sense and correct segment misalignments in our telescope simulator, to again achieve $\sim 10^{-7}$ contrast with an APLC on a static segmented aperture in 360 degree dark hole extending from ~ 4.5 to 12 λ/D, in a 6% band centered at 638 nm. The milestone will include a comparison demonstrating agreement between experimental data and analytical or end-to-end numerical modeling. For example, closed-loop contrast will be compared to predictions based on the experimentally-measured LOWFS sensitivity and on analytic and numerical performance modeling.*

The quantitative performance goal here is identical to Milestone 1; the key difference is starting from an intentionally misaligned segmented aperture (combination of low-order global misalignments and segment-level misalignments).

Correcting these additional static perturbations, as well as additional tip-tilt jitter and low-order aberrations introduced by the ambient turbulence will require combining information from multiple sensors (parametric phase retrieval, tip-tilt sensor, Zernike sensor, e-field focal plane sensing). The main tasks towards this milestone will include:

- Demonstration of Zernike LOWFS sensing on a segmented aperture to measure low-order aberrations introduced both on the continuous DM and on the segmented DM. Evaluate reconstruction accuracy (goal $\sim$ 1 nm rms accuracy) for aberrations amplitudes ranging 1–100 nm peak-to-valley. Sensing will be cross-validated with direct high-precision phase retrieval [Brady et al., 2018]. See section 4.3.3 for more on the specific challenges of extending the Zernike LOWFS to a segmented aperture with APLC.
- Development of analytical error budgets and performance models to quantify sensitivity of this LOWFS to segment modes. Because of the low-pass filtering, segment-to-segment mode will likely be limited to low spatial frequency global modes and some sensitivity to mid spatial frequencies.
- Implementing initial LOWFS control loops and strategies (off-loading to segmented and/or continuous DMs) to achieve closed-loop maintenance of optical alignment for the low-order modes sensed by the LOWFS.
- Higher spatial frequencies not sensed well by the LOWFS will be measured through focal plane wavefront sensing and/or parametric phase retrievals, for synthesis together with LOWFS sensing results.
- Demonstrating closed-loop correction in the presence of injected low-order static disturbances to the segmented telescope simulator (e.g. Zernikes projected onto the segmented DM, and PASTIS modes Leboulleux et al., 2018. We will investigate static disturbances of order 40-60 nm rms. This level is relevant for a mission like LUVOIR for which the total wavefront error (telescope + instrument) is currently set at 38 nm rms [The LUVOIR Team, 2018]. Our testbed calibration has already exceeded this capability (2 nm rms calibrated wavefront error with full circular aperture, and open-loop calibration of Iris-AO DM at 9 nm rms surface error). Therefore it will be straightforward to command larger static aberrations relevant for LUVOIR to explore the capture range of our wavefront sensing and control loops. This approach implicitly assumes any larger initial segment misalignments are sensed and controlled via other means to achieve a diffraction limited beam (rms WFE $\lesssim \lambda/10$), prior to engaging the dark zone control loop. This could for instance be done via a process similar to JWST alignment, which is predicted to achieve 75 nm rms residual after WFSC operating at $\lambda = 2$ μm. [Lightsey et al., 2018])

In parallel with this and supporting this demonstration, we will conduct design and manufacturing the next round of APLC apodizers based on the refined understanding and hardware updates at the end of Year 1. This milestone will be completed by 2020-12-18.

3.3. **TRL 4 system-level dynamic demo (Milestone #2b).** *Demonstrate closed-loop high-contrast wavefront control in the presence of dynamic segment misalignments, in particular by the operation of a LOWFS to sense and correct segment misalignments in our telescope simulator, to again achieve* $\sim 10^{-7}$ *contrast with an APLC on a static segmented aperture in 360 degree dark hole extending from* ~ 4.5 *to 12* λ/D*, in a 6% band centered at 638 nm. Based on the results from currently on-going industry-led studies (e.g. the one led by Ball Aerospace, on which our team is collaborating; Coyle et al., 2018, Pueyo et al., 2019), and in consultation with the Exoplanet Technology Analysis Committee (ExoTAC), we will develop quantitative prescriptions for the relevant*

levels of dynamical drifts to consider in this demonstration. The milestone will include a comparison demonstrating agreement between experimental data and analytical or end-to-end numerical modeling. In particular at that stage the analytic and numerical models will include multiple sensors and temporal errors.

Our final milestone extends into the dynamic regime by introducing slow drifts on the DMs, representative of both global optical instabilities from the telescope and local segment-level instabilities, e.g. from edge-sensors drifts. Faster low-order modes will naturally exist from air turbulence. Multiple integrated control loops will sense and correct these aberrations. In this milestone, we will then seek to demonstrate, in the presence of those temporal drifts, the same contrast performance as above.

Milestone 2b extends the dynamical demonstration to more complex scenarios representative of a real observatory (superposition of low-order drifts and segment-level drifts), requiring more complex control methods. The main tasks towards this milestone will include:

- Refining LOWFS control loops and strategies to achieve continuous, automated, closed-loop maintenance of the dark zone.
- Improving algorithms for instance by implementing optimal control based on the PASTIS analytical model.
- Dynamic tests with operationally realistic scenarios (target / reference star), refining our understanding at the system-level, matching modeling with the data. We will explore a range of drift timescales relevant to the wavefront sensing loop cadence as operating on the testbed (both the dark-zone algorithm loop, and the LOWFS/HOWFS loop). The timescales of interest are respectively lower/comparable/higher than the cadence of each of these loops. We will build on the results of the on-going industry-led studies of observatory stability requirements to relate the timescales of our tests to a mission like LUVOIR. The maximum amplitude of misalignments will be comparable to as in milestone 2a.
- Refinement of high-fidelity numerical models and error budgeting to assess and explain performance behavior.
- Post-processing analysis of operationally realistic scenarios in closed loop (as we did for WFIRST-CGI).
- Implementing HOWFS sensing of high order drifts (software and analysis only, no hardware needed).
- Stretch goal: Implementing HOWFS control based on results of the HOWFS sensing, to further enhance dark zone robustness against higher spatial frequency drifts.

The demonstration of the above will complete by 2021-12-17. We emphasize that the key intellectual output of this demonstration is not simply a specific contrast level but rather an advancement in our *systems-level understanding of the interaction of multiple control systems on a segmented aperture*, as measured by our ability to craft quantitative error budgets for segmented system high contrast performance that are consistent with achieved performance.

Milestone 2b will mark the end of this TDEM program. As part of the exit criteria for TRL-4 (both at the component and system-level) we will include a documented definition of the relevant environments necessary for further advancement at TRL 5 and 6. Based on other work demonstrating TRL-5 of similar technology (e.g. for WFIRST-CGI), we anticipate that the main features of the relevant environment will include vacuum, and the capability for dynamical demonstrations (controlled drifts relevant to a segmented aperture target-mission concept). The provided documentation will set the parameters for these future demonstration by extending the predictions from

the validated analytical / numerical models (e.g. dark zone contrast levels, definition of relevant dynamical drifts on various timescales, etc.) into higher contrast regimes.

4. EXPERIMENT DESCRIPTION

We have developed the HiCAT testbed from the beginning using a system-level goal rather than a purely "contrast-oriented" goal. Figure 4 shows a high-level illustration of the HiCAT current and planned subsystems to enable the technology development program described herein.

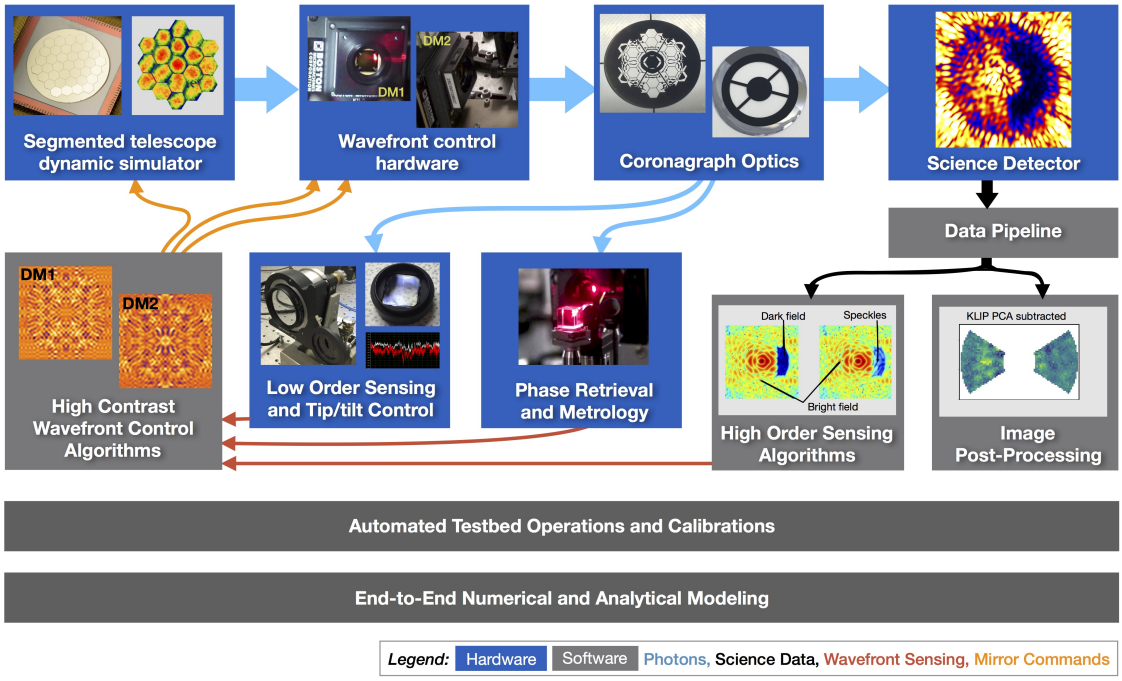

FIGURE 4. The HiCAT experiment plan as a full system demonstration containing hardware and software components integrated together to create and maintain a high-contrast dark zone against perturbations on the spatial and temporal scales relevant for a future space observatory. Boxes indicate the major testbed subsystems either already implemented or planned, and the flows of information between them. Automated operations and high fidelity modeling systems support the functioning and performance optimization of all other components. This TDEM program will support implementations of the low- and high-order sensing (e.g. following N'Diaye et al., 2013b, 2014b and Guyon et al., 2017, Miller et al., 2017), improvements to coronagraph masks, and integration and optimization of all these subsystems (HOWFS and control is a stretch goal).

4.1. **Advancing starlight suppression for segmented apertures at the component level.** Our goal at the component-level is to increase the TRL of APLC designs from TRL 3 to TRL 4. We have recently demonstrated a moderately high contrast dark zone in broadband with a truly segmented aperture ($\sim 10^{-6}$ contrast, in air). The segmented aperture APLC design now meets or exceeds the criteria for TRL 3, and is ready for advancement to higher TRL and higher contrasts (10^{-7} or better). We now will further quantify our understanding of coronagraph mask design optimization, fabrication, and alignment tolerances, and will ground our experiments in thorough end-to-end modeling, to validate our optical error budgets and mature our understanding of trade spaces. As an intermediate (and informal for the TDEM process) milestone, we will contribute our

results to the LUVOIR Science and Technology Definition Team (STDT) final report to the National Academies decadal survey committee, which is due in August 2019. Our first, component-level TRL 4 milestone by the end of 2019 will be in time to inform the Decadal Survey committee as part of their year-long process to assess technology for future NASA missions.

4.2. **Achieving system-level stability for segmented apertures.** Our second objective is demonstrating a closed-loop stabilized dark zone for a LUVOIR-like system, including correction of both natural and artificially simulated dynamic drifts in the system. This will involve the high contrast dark zone algorithms along with sensing information from faster wavefront sensors, similar to what has been done for CGI — but now with the substantial added complication of segmented aberrations to sense and control. We must progress from the current state of the art (two deformable mirror (DM) control) to *three DM sensing and control*, for which there are several possible approaches. Indeed segment-level errors could either be compensated using the downstream continuous DMs, or directly corrected by sending commands back to move the segments. Trade-offs between various methods for sensing and correcting segment-level aberrations need to be understood, along with trade-offs in coronagraph design that can provide more robustness to such misalignments. Through a system-level dynamic demonstration on HiCAT, we will develop (a) more mature wavefront sensing strategies combining multiple sensors, (b) more mature algorithms for high contrast wavefront control including a segmented primary, and (c) improved modeling tools for understanding performance and trade spaces between subsystems. By emphasizing system-level integration starting at an earlier stage (TRL 4), we will be able to bring these improved tools to the Decadal Survey Testbed (DST) to shorten the timescales towards subsequent system-level tests in vacuum.

The key challenge for any operational system is to keep the starlight suppression stable, at the tens of picometer level for 10^{-10} contrast for the most sensitive modes (i.e. pure phase ripples corresponding to speckles in the dark zone), over integration times of hours to days, despite perturbations on faster timescales. Segment-to-segment drift modes, are spatially filtered by the coronagraph and therefore correspond to relaxed levels of stability [Pueyo et al., 2019]; The WFIRST CGI ops concept is to sense and stabilize figure errors from slow thermal drifts as well as line-of-sight pointing jitter using a low-order wavefront sensor (LOWFS) [Shi et al., 2017]. Higher-order wavefront errors are not actively stabilized, but can be removed by post-processing of the science image data — work developed by our group for WFIRST CGI — [Ygouf et al., 2015, 2016], or be small enough to not affect the final contrast.

The current design approach established by the LUVOIR STDT [Bolcar et al., 2017] involves *observatory level metrology systems* to sense and stabilize the large and fast components without relying on starlight to avoid the photon starved regime (e.g. using edge sensors, laser truss, or laser guide star; Feinberg et al., 2017, Coyle et al., 2018, Clark et al., 2018). But non-common-path perturbations between the metrology and science channels will result in long timescales drifts. In addition to the need for a LOWFS and science data post-processing (as for WFIRST CGI), sensing these slow drifts will require a high-order wavefront sensor (HOWFS) on LUVOIR. We will integrate all these components on HiCAT for a full-system demonstration.

4.3. **Detailed Experimental plans.**

4.3.1. *Developing Numerical and Analytical Modeling Methods.* We will ground our experiments in thorough end-to-end modeling, to validate our optical error budgets, provide quantitative performance predictions for the TRL milestones, and mature our understanding of trade spaces. Both

numerical and analytical/semi-analytical modeling tools are needed. Rigorous end-to-end numerical optical propagation models are needed to derive interaction matrices, validate algorithms, and cross-check our understanding of testbed performance limits. Analytical models, which can be computed typically orders of magnitude faster, allow rapid tolerancing for error budgets, exploration of trade spaces, and fast simulations of dynamic control loops.

We have already completed our "medium-fidelity simulator" — i.e. a simulator based on a simplified optical system (APLC, three DMs, overall combined wavefront error) but without explicit propagation through the entire optical train with every optical surface. This simulator is sufficient for calculating our wavefront control interaction matrices, and for developing our software offline without the need to interface directly to the actual hardware, since it has been built to use the same interfaces (DM commands, and identical format of output FITS files). Figure 5 shows an example simulation, and Figure 7 shows a recent dark zone enabled by control matrices generated from the simulator, and using control software developed offline using the simulator.

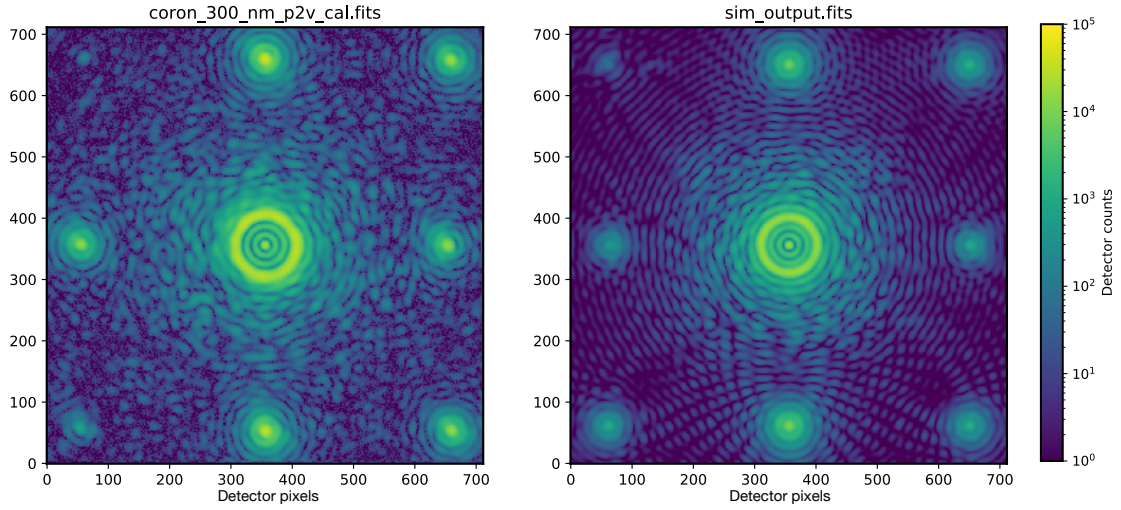

FIGURE 5. Example output from our medium fidelity simulator. This example is from a test of the COFFEE phase retrieval algorithm [Paul et al., 2013] with probe patterns applied to the DM, prior to generation of a dark hole. *Left:* Actual testbed image. *Right:* Simulated image for the same configuration and simulated DM settings. The overall morphology and many details are in good agreement. The main difference is the simulated image here has lower speckle halo at wide separations (corresponding to high spatial frequencies well outside of the dark zone control frequencies, and thus less of a priority for inclusion in the simulator thus far.) Note the different intensities of the satellite spots caused by the DM actuator print-through. These asymmetries arise due to Fresnel propagation between the two DMs, which at this time were slightly misaligned in translation by about 0.2 actuator spacings. The details of this alignment and the resulting diffractive effects are reasonably well reproduced in the simulator.

The high fidelity end-to-end model will be developed in collaboration with the GSFC sub-team, Ball Aerospace, and the University of Rochester. Work has already started at GSFC and Rochester for a high fidelity model of LUVOIR's coronagraph [Juanola-Parramon et al., 2018] using rigorous diffractive modeling tools [Krist et al., 2016, Perrin et al., 2016]. We will adapt the same tools to construct a high fidelity model of HiCAT, integrated with the testbed control software and calibration systems so as to allow efficient automated numerical modeling of experiment setups.

For rapid modeling and tolerancing studies, we will also continue the development of an analytical model that relates final contrast directly to segment-level wavefront errors (Pair-based Analytical model for Segmented Telescopes Imaging from Space, PASTIS; Leboulleux et al., 2018). A key advantage of this new method is that its matrix-based formalism allows decomposition into aberration eigenmodes that can be ordered by their impacts on contrast. Analytical inversions can directly derive allowable amplitudes per mode to achieve a given target contrast. (See Figure 6). We will investigate the application of PASTIS for developing realistic error budgets, stability analyses, and modal control algorithms with more optimal noise properties.

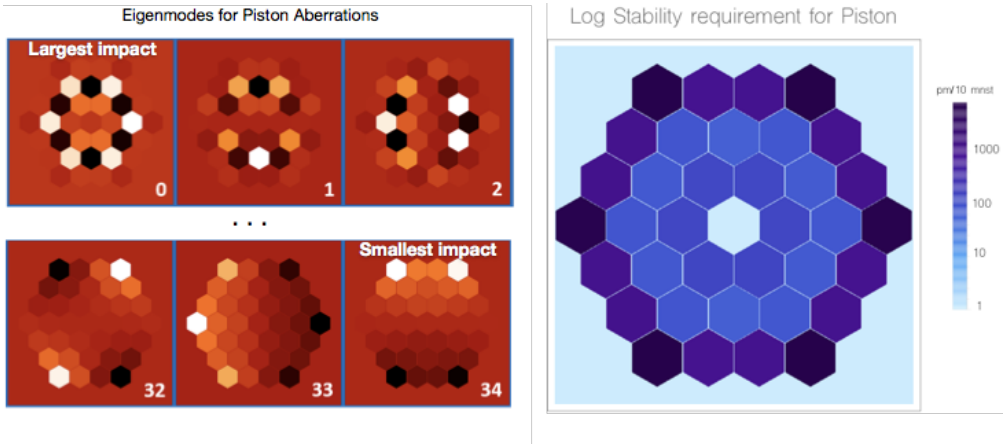

FIGURE 6. Examples of wavefront singular modes computed using the PASTIS analytical model [Leboulleux et al., 2018]. *Left*: Eigenmodes on the primary mirror for segment-level piston errors. Typically alternating "hexagonal checkerboard" patterns have the most adverse effects upon contrast. This knowledge can help put constraints on the opto-mechanical design (e.g. back plane structures designed to attenuate the most sensitive modes), and also designing the coronagraph for robustness to these modes. PASTIS modes also exist for any other segment-level aberrations, such as tip, tilt and astigmatism which would be typically observed on a segmented primary mirror. We also plan to use these modes to for modal wavefront control. *Right*: Derived stability requirement (expressed as acceptable wavefront drift per 10 minutes) to achieve 10^{-10} dark zone contrast with stability of 10^{-11} [Pueyo et al., 2019]. This wavefront stability map combines the drift tolerance calculated for each PASTIS mode (shown here for piston only, but the method is applicable to other PASTIS modes). The calculation assumes a star of magnitude 5 over a 16 hour sequence, in the presence of continuous wavefront sensing and control assuming residuals are driven by photon noise on the wavefront sensor only. We assume that other sources of noise in the sensor (read noise, dark current) are negligible, and that the control is perfect (no lag, unit gain, modes perfectly controllable).

4.3.2. *Implementing more advanced wavefront control algorithms.* Our initial wavefront control strategy was based on the speckle nulling approach which is model independent, but highly dependent on calibration. We are now transitioning to model-dependent algorithms that were developed by our team investigators [Pueyo et al., 2009, Mazoyer et al., 2018a,b], which have recently become functional by the beginning of the TDEM technical work. See Figure 7 for a recent dark zone achieved using the model-dependent stroke minimization algorithm controlling both phase and amplitude aberrations on HiCAT. As part of our system-level demonstration, we plan to implement more recent approaches that are particularly promising to relax stability constraints [Riggs et al., 2016, Sun et al., 2017, Pogorelyuk and Kasdin, 2019]. In this TDEM program we will assess how well these existing algorithms work in the segmented context, and develop integrated software for segment control alongside dark zone control. The high-fidelity model we will be developing

in parallel will allow us to cross check between performance and expectations. This will be a key ingredient in maturing contrast error budgets and related systems engineering tools.

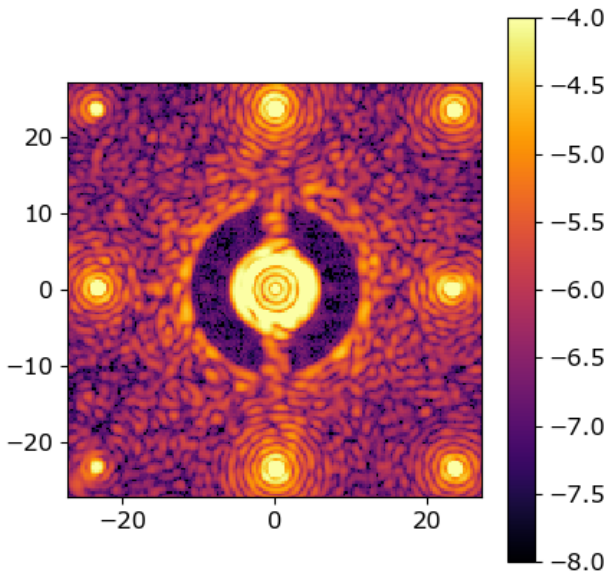

FIGURE 7. The first double-sided dark zone achieved on HiCAT, using stroke minimization wavefront control along with pairwise probes for sensing the electric field in the focal plane (image contrast shown in log scale). This demonstration is for a monolithic circular aperture with unoptimized classical Lyot coronagraph, not yet the segmented aperture nor APLC as we will demonstrate in this TDEM. This dark zone was achieved in our very first instance of running the dual-DM stroke min controller on HiCAT, with just a single afternoon on the testbed plus unattended scripted operation into the evening. The dual-DM control software and pairwise probe software were prototyped and debugged on the medium fidelity simulator, and ran correctly on the hardware on the first try. The quality of the dark zone here implicitly shows already fairly good consistency between model and hardware, since it was achieved via a model-dependent algorithm using wavefront control interaction matrices generated using our simulator. This demonstration on a monolithic aperture provides a foundation for the subsequent planned demonstrations on segmented apertures with HiCAT. The level of contrast and background observed in the darkest areas are sufficiently low as to be compatible with operation below 10^{-7} contrast, which validates the capabilities of our infrastructure to conduct the stated work.

4.3.3. *Implementing Low Order Sensing and Control.* We will extend the ability of HiCAT to work in the dynamical regime with the implementation of a Zernike LOWFS N'Diaye et al., 2013b, 2014b.), in close collaboration with the University of Nice and Laboratoire d'Astrophysique de Marseille, who provided the Zernike phase mask. We have already implemented a prototype LOWFS subsystem on our secondary testbed, and validated the general behavior of our Zernike sensor, as well as its overall optical design (albeit with cheap off the shelf off-axis parabolas). In addition to the Zernike sensor, the LOWFS subsystem includes a target acquisition camera that re-images the coronagraphic hole and allows precise centering of the star at the center of the masks, and a quad-cell sensor to drive our piezo tip-tilt controller. Of course, the Zernike sensor could also be used to drive tip-tilt and the two sensor options will be studied once in operation. The current baseline plan is to control tip-tilt using our quad-cell sensor, and use the Zernike for the higher-order modes — this should have the advantage of maximizing the dynamic range of the

Zernike sensor. Final optics are now in procurement and will be implemented on HiCAT in the first few months of the TDEM. An important part of the TDEM work will be to understand the effects of spatial filtering by the focal plane mask (low-pass filtering), since our Zernike wavefront sensor is using the light limited to the core of the PSF that traverses the focal plane mask, which is a circular hole in a mirror (see Figure 2 third panel, and Figure 8). In addition, our Zernike sensor will also have to operate in the presence of an apodized and segmented pupil, which is a new range of application for this type of sensor. Currently a team of three undergraduate students is dedicated to the implementation of the LOWFS infrastructure, as part of their Senior Design class in Mechanical Engineering and is on-track to complete with the 2019 academic year. This will be followed by dedicated student and graduate student work both at STScI and University of Nice.

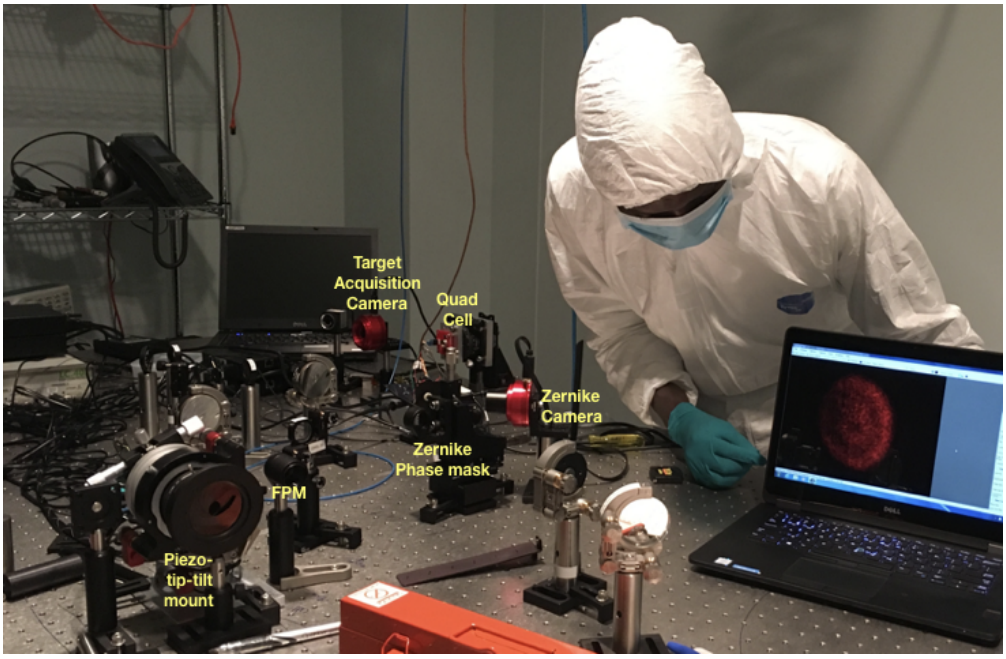

FIGURE 8. Prototype low-order wavefront sensor (LOWFS) subsystem, on a separate table and reproducing the same optical layout as planned on HiCAT, albeit with cheap off-the-shelf optics. The piezo tip-tilt mount is partially masked by a manual iris that was adjusted to have the same f-ratio at the focal plane mask (FPM) as on HiCAT. In addition to the Zernike sensor, a quad-cell is used to control the tip-tilt stage, and a target acquisition camera re-images the back of the FPM hole, to allow for high-precision centering of the star with respect to the FPM. Collaborator N'Diaye is showing the Zernike sensor image on the screen where ringing due to the spatial filtering by the FPM is clearly visible. A team of undergraduate students is dedicated to the operational aspects of this testbed to enable autonomous target acquisition for HiCAT .

4.3.4. *Implementing Dynamic Tests by Introducing Perturbations.* We will extend the operations in the *dynamic* regime by introducing temporal drifts on the segmented DM that are representative of small observatory-level deformations and drifts. We will begin with simple low-order Zernike perturbations (e.g. focus, astigmatism, coma), and then directly investigate the propagation through the system of the singular modes derived by the PASTIS model. We will study how these drifts can be sensed and controlled and will investigate the influence of the wavefront perturbation frequency on the system.

4.3.5. *Implementing High-Order Wavefront Sensing.* To sense segment-level aberrations we will explore recent concepts for HOWFS implementations that can work directly on science focal plane data, in particular out-of-band speckle field or linear dark-hole correction [Guyon et al., 2017, Miller et al., 2017]. On a flight mission, such algorithms may require a dedicated sensor because of dynamic range limitations between the dark and bright zones. For HiCAT, we can implement them directly with our existing hardware, thanks to fast exposure times with our CMOS cameras. After completion and integration of the LOWFS we will explore high-order sensing aspects (e.g. relating a modal drift to the HOWFS signal). Implementation of closed-loop high-order control is a stretch goal for time planned at the end of the project.

4.3.6. *Assessing Operations as Part of System-level Studies.* Our system-level demonstration will in part rely on the implementation of more realistic simulated operations. We have already well advanced in this direction with our calibration suite and autonomous infrastructure, but will continue to strive towards this goal, which we believe is key to system-level understanding. For example, we will investigate autonomous operations to include target acquisition, phase retrieval wavefront pre-calibration, and multiple pupils alignment (segmented primary mirror,apodizer, and Lyot Stop) and registration to the DMs. We periodically conduct a large ensemble of automated routine calibration tasks (e.g. including source flux calibrations, auto-focus, position of the detector sub-array, plate scale, contrast normalization). to build a trending database that will be used for identification of drifts, component degradation, and/or alignment errors. This information will be key to understanding factors limiting performance and validating our models.

4.3.7. *Implementing Post-processing.* Our group has led major advances in high-contrast post-processing techniques, in particular with our Principal Component Analysis algorithm "KLIP" [Soummer et al., 2012, Pueyo, 2016] which is now ubiquitous in high-contrast observations. We led the pre-phase-A post-processing analysis work for WFIRST CGI [Ygouf et al., 2015, 2016]. By analyzing long time-series ($\sim$ 12h) of images acquired on the WFIRST Optical Mask Coronagraph (OMC) testbed at JPL, we demonstrated post-processing contrast gains of 7–30 depending on the coronagraph sequence and image correlation level. Such dynamic drift experiments are exactly what we plan to conduct with HiCAT (for both natural and induced drifts). In that case, the ability to generate realistic operational scenarios on long time scales (e.g., involving a science target and reference star separated by an observatory slew) was limited by time constraints and operations cost of the OMC. That experience reinforces the advantage of our highly automated approach to HiCAT operations in ambient conditions, making very long observing sequences straightforward. We will employ state-of-the-art post-processing as part of the dynamic experiments on HiCAT, implemented in our automated data reduction system.

4.3.8. *Segmented aperture simulator.* Our segmented aperture relies on using a segmented DM manufactured by the company Iris-AO, which recently ceased operations. Fortunately, the company had already delivered to us two fully-functioning systems (DM and controller), one of which we reserve as a spare. The current Iris-AO DM on HiCAT is of excellent surface quality with open loop surface error of 9 nm rms [Soummer et al., 2018]. In addition we also have two engineering-grade DMs (not all actuators operable, but both have "JWST-like" sub-regions of 18 contiguous operable segments, which would still enable our key demonstration goals in the unlikely event that both of our science-grade DMs were to become unavailable). We consider that the risks on our project plans are appropriately mitigated by these existing spare deformable mirrors on hand.

Our lab infrastructure also includes continuous automated monitoring of environmental factors including humidity, temperature, and power to ensure the safe operation of high-value electronics including both the segmented and continuous DMs.

4.3.9. *Path towards future demonstrations in vacuum.* In parallel with the above we will also continue our collaborations with the DST team, and others on e.g. the HabEx and LUVOIR study teams, towards the collective future goal of a vacuum demonstration of even higher contrast dark zones on segmented apertures. As of this writing, future plans on the DST are in flux, both in terms of experiment choices/priorities and available hardware (e.g. actual segmented DM versus segmented aperture mask only). As these plans are refined, our team intends to remain engaged in supporting these activities for technology maturation in support of the HabEx and LUVOIR mission concepts.

5. Data Measurement and Analysis

5.1. **Definitions.**

5.1.1. *Raw and Calibrated image.* Raw images are processed through a standard pipeline to produce calibrated images with standard tasks such as background subtraction, deviant pixels correction, image registration and stacking, final rebinning and exporting to FITS files with metadata information.

5.1.2. *DM flats and calibrated Zernike aberrations.* Our deformable mirrors have been calibrated in closed-loop in front of our Fizeau interferometer, both to produce "flat maps" as well as calibrated Zernike maps up to the Spherical aberration for a range of amplitudes. Each DM has been calibrated independently.

5.1.3. *Star.* The simulated star is obtained by a single mode fiber direct output. We have plans to upgrade this fiber launch using a pinhole following the example of what has been done at JPL. The input of the fiber can be fed either by a laser diode at 638nm for monochromatic operations, and for broadband operations, we can choose between a PhotonETC monochromator coupled with a super-continuum laser to produce adjustable 1% narrow band images, and with a filter-wheel based filter assembly coupled with the same super-continuum laser. The filter-wheel assembly allows higher flux than the tunable monochromator, but is limited to our existing filter set.

5.1.4. *Monochromatic and broadband.* Monochromatic refers to operations using our laser diode at 638nm. Broadband refers either to composite broadband from stacking narrow band images using the tunable monochromator, or directly broadband images using a single broadband filter using our filter-wheel assembly.

5.1.5. *Contrast value.* For consistency across the various TDEM programs, we align our contrast definition to the approach followed e.g. by Serabyn [2010, 2014]), which is also consistent with other past TDEMs. The star is aligned on the coronagraph focal plane mask and Lyot stop aligned. An image is taken of the coronagraph field (the suppressed star and surrounding speckle field). The image is normalized to the peak value of the star brightness using the calibration ladder defined in Section 5.1.7 below. The contrast will be calculated for an annulus (or half-annulus) between the IWA and OWA in the speckle field.

5.1.6. *Average and Mean contrast, standard deviation.* These terms are also aligned with the definitions from the TDEM white paper by Serabyn [2010, 2014], where "average contrast" refers to the spatial average over the dark zone, whereas "mean contrast" refers to averaging of individual average contrast values in a sequence of images. Quoting Serabyn [2014]: *the "standard deviation" σ_{meas} for an individual measurement of the average contrast value c_i is given as usual by: $\sigma_{meas} = \sqrt{\sum_{i=1}^{n} \frac{(c_i - \hat{c})^2}{n-1}}$. The uncertainty in the mean contrast $\hat{c}$ is then given by $\sigma_{mean} = \sigma_{meas}/\sqrt{n}$. There is also a contribution to the uncertainty from the independently-determined photometry error, σ_{phot}. The net standard deviation is thus $\sigma = \sqrt{\sigma_{mean}^2 + \sigma_{phot}^2}$*

5.1.7. *Measurement of star brightness.* Our contrast calibration (regardless of the contrast metric) has to be relative to a direct star image (i.e. where the occulting FPM has been removed, but everything else is unchanged, as to represent the PSF of a planet companion. The use of CMOS cameras with very short exposure time facilitates the calibration ladder. At the moment the calibration relies on direct short exposures of the star and long exposures in coronagraphic mode. We also plan to implement well-calibrated density filters to attenuate the direct image using a motorized flip mount and improve the calibration ladder to avoid the shortest exposure times, which carry more relative uncertainty.

5.1.8. *Measurement of the focal plane scale.* IWA and OWA values are expressed in units of $lambda/D$ where D is either the apodizer diameter, or the Lyot Stop. The "sampling" value is by definition the number of pixels by $lambda/D$. Focal plane calibrations rely on several approaches: detection of the cut-off frequency in the Modulus Transfer Function (MTF), and injection of known phase ripples on the DM with or without Lyot stop, as well as information from direct pupil diameter measurements.

5.1.9. *Statistical Confidence.* Here again, for consistency with other TDEM work, we quote the definition used in the TDEM white paper by Serabyn [2010, 2014].

For contrast values that have a Gaussian distribution about the mean contrast, the statistical confidence that the mean contrast $\hat{c}$ is less than some value c_0 is given by

$$conf(z < t) = \frac{1}{\sqrt{2\pi}} \int_{\infty}^{t} e^{-z^2/2} dz = \frac{1}{2} + \frac{1}{\sqrt{2\pi}} \int_{0}^{t} e^{-z^2/2} dz \quad (1)$$

where $t = (c_0 - \hat{c})/\sigma$. Thus, as $\hat{c} = c_0 = t\sigma$, meeting a milestone contrast target c_0 with the desired confidence level requires the final measured mean contrast for a given run, $\hat{c}$, to be lower than the target contrast c_0 by t standard deviations. The Gaussian integral is widely tabulated, and $conf = 0.9$ implies $t = 1.28$. Thus, for 90% confidence, $\hat{c} = c_0 = 1.28\sigma$, i.e. the measured $\hat{c}$ must be smaller than the target c_0 by 1.28σ.

5.2. **Milestone demonstration procedure.** Operations start with flat DMs, and with the FPM out of the beam (direct image, acquired for contrast calibration). After initial autonomous target acquisition, the wavefront control iterations will proceed until convergence is attained. The final contrast field is acquired. Additional experiments are then conducted either by maintaining to the correction and perturbing the system to study tolerances and robustness, or by adding controlled drifts for the dynamical study.

Since our investigation place emphasis on the system-level demonstration with a high-level of infrastructure with autonomous experiment scripts, the milestones must be satisfied on three separate occasions with a complete reset of the system between each demonstration (according to the process followed by other past TDEMs, e.g. Serabyn [2010].

5.3. **Milestone Data Package.**

- A narrative report that explains how the milestone was met, how experiments were conducted, hardware state and configuration for that experiment, and an evaluation of the statistical significance of the result.
- Calibrated contrast images, direct images, contrast plots and figures, and synthetic validation images with injected fake planets.
- detailed description of algorithm and methods used to allow for independent assessment of the delivered data.

6. SUCCESS CRITERION

Unless specified as monochromatic, experiments will consist of broadband ($\sim 6\%$, with goal $\sim 10\%$) observations around the 638 nm wavelength, which is the central design wavelength. The nominal dark zone will be established between 4.5 and 12 λ/D, where D refers to the circumscribed diameter of the apodizer for the APLC. The contrast requirement for each milestone is set at $\sim 10^{-7}$ based on the assumption of at least $10\times$ improvement over completed initial tests. In consistency with other TDEMs [Serabyn, 2010, 2014], milestones contrast will correspond to a confidence level of 90% or better, under the assumption that contrasts have a Gaussian distribution about the mean.

Performance better than that may also be possible; we designed the HiCAT testbed (optical design, surface quality, and APLC masks) to reach 10^{-8} in theory. Of course, operating in air, HiCAT is limited by more environmental instabilities compared to a vacuum experiment. We have quantified environmental disturbances using rapid imaging (~ 300 fps) and accelerometers. Most of the power resides in low-order aberrations at very low frequency (below 10 Hz). This is favorable for a exploration of system-level control using a LOWFS without the need for heavy-duty piezo hardware or serious real-time computing. Furthermore, the Paris high-contrast testbed has demonstrated 10^{-8} contrast in air [Delorme et al., 2016]. Given these facts we expect that contrasts to 10^{-8} (including post-processing) should be achievable with HiCAT, especially since developing the systems control methods to handle a dynamic environment is a key part of our goal. However given the remaining uncertainties in the ambient environment we choose for now to set a relatively conservative milestone requirement of $\sim 10^{-7}$, while still pursuing a goal of $\sim 10^{-8}$.

Very recent experimental tests (April 2019) have confirmed that the testbed environmental instability/dynamics noise at high spatial frequencies and the incoherent background noise are both sufficiently low as to be compatible with operation below 10^{-7} contrast (e.g. Figure 7). Work to quantify these terms and others into an as-built system contrast budget is actively ongoing. Currently, correcting for the dominant low frequency tip/tilt drifts is done via shift-and-add coaddition of many short exposures, which comes with inefficient high overheads, but tip/tilt drifts will be actively controlled once the LOWFS becomes operational over summer 2019.

Because the central goals of this project are focused on advancing the understanding of the complete dynamical system, and because our separate SCDA study has already demonstrated that APLC coronagraph designs can achieve 10^{-10}, we consider that the success criterion should not depend strictly on pushing the achieved value of contrast to any particular value such as 10^{-8}. Rather the key output is a quantitative understanding of the contrast error budget and limiting factors. Each milestone will therefore be accompanied with appropriate modeling to reproduce the measured performance and associated tolerances or sensitivities. The fidelity of these models should be as important a success metric as the specific contrast levels achieved.

7. SCHEDULE

7.1. **Precursor work.** Supported by existing funding, we have been preparing for this TDEM work plan along the following specific steps — reported here as written in the original TDEM proposal written in February 2018, with current status updated added in italics. These efforts are generally on track at this point in time:

- Systematic analysis of current performance limitations and implementation of enhancements to increase robustness and performance. *Completed. Improvement of several mounts, new pupil camera setup, new pupil mount installed.*
- Refinement of calibration tools, specifically phase retrieval through apodizers and segmented apertures. *On track. COFFEE algorithm reconstruction of segmented aperture completed (Paul et al., 2013; Leboulleux et al. in prep), Parametric phase retrieval extended to apodized configuration under development with successful low-order reconstruction [Brady et al., 2018].*
- Integration of a two-DM stroke minimization dark zone algorithm. *Completed. Operational as of April 2019. See Figure 7.*
- Improvement of the operations of our tip-tilt stage. *Completed. This year's JHU Senior Design undergrad team completed an operational system including autonomous target acquisition, and closed-loop tip-tilt with high-precision centering of the beam with respect to the focal plane mask. This tip-tilt system will be transferred from the development bench to main testbed during summer 2019.*
- Beginning assembly of the LOWFS. *On track. Completed end-to-end qualitative demonstration with all hardware on table and cheap placeholder optics. Final high-precision optics to be delivered in May 2019.*
- Design and manufacture of the next iteration of carbon nanotube apodizer masks. *Completed. New set of apodizers in hand, including compensation for foreshortening due to angle of attack; already working on next round of designs.*

7.2. **Work under this TDEM.** The technology development work plan will start upon approval of this white paper, and will represent a smooth continuation of our current efforts under other funding sources.

Our goal is to reach a *component-level* TRL 4 demonstration of the APLC coronagraph with a segmented aperture by the end of the first year (milestone 1), and *system-level* TRL 4 demonstration by the end of the third year (dynamic perturbations; milestone 2b), with a preliminary system-level intermediate milestone (2a) at the end of the second year (static perturbations sensed by LOWFS). The planned schedule is presented in Figure 9. Many individual tasks support both milestones and are phased accordingly.

More details on team organization and work breakdown are provided in our TDEM proposal document and are not repeated here. Efforts are split among four major threads (Optics & WFSC, Modeling, Software, and Optomechanics), each with identified lead(s). All critical tasks needed to meet the milestones will be conducted by the core group of Baltimore-based team members, who are all co-located in STScI's Makidon lab, or nearby on the JHU campus. Our core group, particularly the leadership team, has been in place for 3+ years. The subteam leads are responsible for coordinating with our external collaborators on those topics. Collaborations with JPL, GSFC, and France bring enhancements to the scope (e.g. collaboration on end-to-end modeling tools with LUVOIR, additional analytical modeling tools, collaborations on WFS&C algorithms), but do not introduce any critical-path dependencies.

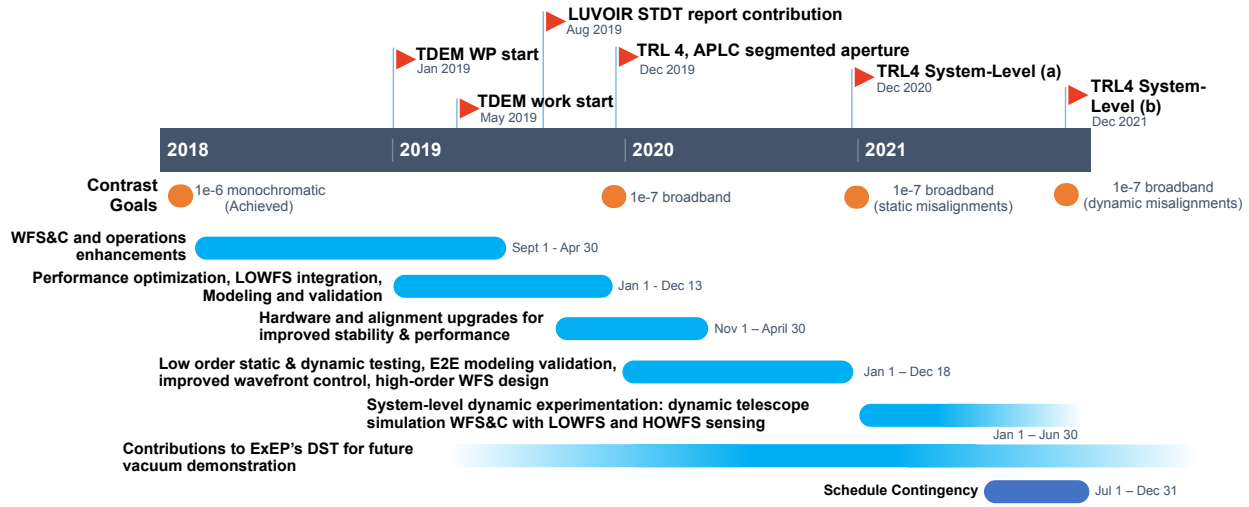

FIGURE 9. Our planned activities for this TDEM over its three-year duration. With on-going Decadal Survey mission studies, we will first contribute to the LUVOIR STDT final report (August 2019). Our component-level TRL 4 milestone demonstrates the APLC coronagraph with segmented aperture by the end of 2019. The system-level milestones are split in two parts, a first part by the end of 2020 with static disturbances, and the second part with dynamic disturbances and operationally realistic scenarios by the end of the project. Our work plan includes staggered development of each component. For example a preliminary implementation of the Zernike wavefront sensor has already been validated. We dedicate a significant amount of time around the first milestone for hardware upgrades, that will be determined based on the performance and limitations observed at this milestone. We also include a six-month schedule contingency at the end of the project.

REFERENCES

K. Balasubramanian, A. J. E. Riggs, E. Cady, V. White, K. Yee, D. Wilson, P. Echternach, R. Muller, C. Mejia Prada, B.-J. Seo, F. Shi, D. Ryan, S. Fregoso, J. Metzman, and R. C. Wilson. Fabrication of coronagraph masks and laboratory scale star-shade masks: characteristics, defects, and performance. In *Society of Photo-Optical Instrumentation Engineers (SPIE) Conference Series*, volume 10400 of *Society of Photo-Optical Instrumentation Engineers (SPIE) Conference Series*, page 104000C, September 2017. doi: 10.1117/12.2274059.

M. R. Bolcar, S. Aloezos, V. T. Bly, C. Collins, J. Crooke, C. D. Dressing, L. Fantano, L. D. Feinberg, K. France, G. Gochar, Q. Gong, J. E. Hylan, A. Jones, I. Linares, M. Postman, L. Pueyo, A. Roberge, L. Sacks, S. Tompkins, and G. West. The Large UV/Optical/Infrared Surveyor (LUVOIR): Decadal Mission concept design update. In *Society of Photo-Optical Instrumentation Engineers (SPIE) Conference Series*, volume 10398 of *Society of Photo-Optical Instrumentation Engineers (SPIE) Conference Series*, page 1039809, September 2017. doi: 10.1117/12.2273848.

G. R. Brady, C. Moriarty, P. Petrone, I. Laginja, K. Brooks, T. Comeau, L. Leboulleux, and R. Soummer. Phase-retrieval-based wavefront metrology for high contrast coronagraphy. In *Space Telescopes and Instrumentation 2018: Optical, Infrared, and Millimeter Wave*, volume 10698 of *Society of Photo-Optical Instrumentation Engineers (SPIE) Conference Series*, page 106986I, July 2018. doi: 10.1117/12.2314368.

E. Cady, C. M. Prada, X. An, K. Balasubramanian, R. Diaz, N. J. Kasdin, B. Kern, A. Kuhnert, B. Nemati, I. Poberezhskiy, A. J. Eldorado Riggs, R. Zimmer, and N. Zimmerman. Demonstration of high contrast with an obscured aperture with the WFIRST-AFTA shaped pupil coronagraph. *Journal of Astronomical Telescopes, Instruments, and Systems*, 2(1):011004, January 2016. doi: 10.1117/1.JATIS.2.1.011004.

E. Cady, K. Balasubramanian, J. Gersh-Range, J. Kasdin, B. Kern, R. Lam, C. Mejia Prada, D. Moody, K. Patterson, I. Poberezhskiy, A. J. E. Riggs, B.-J. Seo, F. Shi, H. Tang, J. Trauger, H. Zhou, and N. Zimmerman. Shaped pupil coronagraphy for WFIRST: high-contrast broadband testbed demonstration. In *Society of Photo-Optical Instrumentation Engineers (SPIE) Conference Series*, volume 10400 of *Society of Photo-Optical Instrumentation Engineers (SPIE) Conference Series*, page 104000E, September 2017. doi: 10.1117/12.2272834.

J. R. Clark, A. Carlton, E. S. Douglas, J. R. Males, J. Lumbres, L. Feinberg, O. Guyon, W. Marlow, and K. L. Cahoy. Capabilities of a Laser Guide Star for a Large Segmented Space Telescope. In *American Astronomical Society Meeting Abstracts #231*, volume 231 of *American Astronomical Society Meeting Abstracts*, page 419.08, January 2018.

L. E. Coyle, J. S. Knight, and M. Adkins. Edge sensor concept for segment stabilization. In *Space Telescopes and Instrumentation 2018: Optical, Infrared, and Millimeter Wave*, volume 10698 of *Society of Photo-Optical Instrumentation Engineers (SPIE) Conference Series*, page 1069869, July 2018. doi: 10.1117/12.2312224.

J. R. Delorme, M. N'Diaye, R. Galicher, K. Dohlen, P. Baudoz, A. Caillat, G. Rousset, R. Soummer, and O. Dupuis. Laboratory validation of the dual-zone phase mask coronagraph in broadband light at the high-contrast imaging THD testbed. *Astron. & Astrophys.*, 592:A119, August 2016. doi: 10.1051/0004-6361/201628587.

L. Feinberg, M. Bolcar, S. Knight, and D. Redding. Ultra-stable segmented telescope sensing and control architecture. In *Society of Photo-Optical Instrumentation Engineers (SPIE) Conference Series*, volume 10398 of *Society of Photo-Optical Instrumentation Engineers (SPIE) Conference Series*, page 103980E, September 2017. doi: 10.1117/12.2272810.

L. D. Feinberg, A. Jones, G. Mosier, N. Rioux, D. Redding, and M. Kienlen. A cost-effective and serviceable ATLAST 9.2m telescope architecture. In *Society of Photo-Optical Instrumentation Engineers (SPIE) Conference Series*, volume 9143 of *Society of Photo-Optical Instrumentation Engineers (SPIE) Conference Series*, page 16, August 2014. doi: 10.1117/12.2054915.

R. Goullioud, F. Zhao, H. Tang, and J. Wu. The WFIRST-AFTA coronagraph design update. In *Society of Photo-Optical Instrumentation Engineers (SPIE) Conference Series*, volume 9143 of *Society of Photo-Optical Instrumentation Engineers (SPIE) Conference Series*, page 0, August 2014. doi: 10.1117/12.2057393.

O. Guyon, K. Miller, J. Males, R. Belikov, and B. Kern. Spectral Linear Dark Field Control: Stabilizing Deep Contrast for Exoplanet Imaging Using out-of-band Speckle Field. *ArXiv e-prints*, June 2017.

J. G. Hagopian, S. A. Getty, M. Quijada, J. Tveekrem, R. Shiri, P. Roman, J. Butler, G. Georgiev, J. Livas, C. Hunt, A. Maldonado, S. Talapatra, X. Zhang, S. J. Papadakis, A. H. Monica, and D. Deglau. Multiwalled carbon nanotubes for stray light suppression in space flight instruments. In *Carbon Nanotubes, Graphene, and Associated Devices III*, volume 7761 of *Proc. SPIE*, page 77610F, August 2010. doi: 10.1117/12.864386.

R. Juanola-Parramon, N. Zimmerman, M. R. Bolcar, M. Rizzo, and A. Roberge. Modelling exoplanet detection with the LUVOIR Coronagraph: aberration sensitivity and error tolerances. In *American Astronomical Society Meeting Abstracts #231*, volume 231 of *American Astronomical Society Meeting Abstracts*, page 246.37, January 2018.

J. Krist, B. Nemati, and B. Mennesson. Numerical modeling of the proposed WFIRST-AFTA coronagraphs and their predicted performances. *Journal of Astronomical Telescopes, Instruments, and Systems*, 2(1):011003, January 2016. doi: 10.1117/1.JATIS.2.1.011003.

L. Leboulleux, M. N'Diaye, A. J. E. Riggs, S. Egron, J. Mazoyer, L. Pueyo, E. Choquet, M. D. Perrin, J. Kasdin, J.-F. Sauvage, T. Fusco, and R. Soummer. High-contrast imager for Complex Aperture Telescopes (HiCAT). 4. Status and wavefront control development. In *Space Telescopes and Instrumentation 2016: Optical, Infrared, and Millimeter Wave*, volume 9904 of *Proc. SPIE*, page 99043C, July 2016. doi: 10.1117/12.2233640.

L. Leboulleux, M. N'Diaye, J. Mazoyer, L. Pueyo, M. Perrin, S. Egron, E. Choquet, J.-F. Sauvage, T. Fusco, and R. Soummer. Comparison of wavefront control algorithms and first results on the high-contrast imager for complex aperture telescopes (hicat) testbed. In *Society of Photo-Optical Instrumentation Engineers (SPIE) Conference Series*, volume 10562 of *Society of Photo-Optical Instrumentation Engineers (SPIE) Conference Series*, page 105622Z, September 2017. doi: 10.1117/12.2296154.

L. Leboulleux, J.-F. Sauvage, L. A. Pueyo, T. Fusco, R. Soummer, J. Mazoyer, A. Sivaramakrishnan, M. N'Diaye, and O. Fauvarque. Pair-based Analytical model for Segmented Telescopes Imaging from Space for sensitivity analysis. *Journal of Astronomical Telescopes, Instruments, and Systems*, 4(3):035002, July 2018. doi: 10.1117/1.JATIS.4.3.035002.

Paul A. Lightsey, J. Scott Knight, Allison Barto, Koby Smith, Taylor Chonis, Laura Coyle, Scott Acton, Scott Rohrbach, Kim Mehalick, Lee Feinberg, William Hayden, Charles Atkinson, Conrad Wells, and James Hadaway. James Webb Space Telescope optical performance predictions post cryogenic vacuum tests. In *Society of Photo-Optical Instrumentation Engineers (SPIE) Conference Series*, volume 10698, page 1069804, Jul 2018. doi: 10.1117/12.2312276.

J. Mazoyer, L. Pueyo, M. N'Diaye, K. Fogarty, N. Zimmerman, L. Leboulleux, K. E. St. Laurent, R. Soummer, S. Shaklan, and C. Norman. Active Correction of Aperture Discontinuities-Optimized Stroke Minimization. I. A New Adaptive Interaction Matrix Algorithm. *Astronomical Journal*, 155:7, January 2018a. doi: 10.3847/1538-3881/aa91cf.

J. Mazoyer, L. Pueyo, M. N'Diaye, K. Fogarty, N. Zimmerman, R. Soummer, S. Shaklan, and C. Norman. Active Correction of Aperture Discontinuities-Optimized Stroke Minimization. II. Optimization for Future Missions. *Astronomical Journal*, 155:8, January 2018b. doi: 10.3847/1538-3881/aa91d7.

K. Miller, O. Guyon, and J. Males. Spatial linear dark field control: stabilizing deep contrast for exoplanet imaging using bright speckles. *Journal of Astronomical Telescopes, Instruments, and Systems*, 3(4):049002, October 2017. doi: 10.1117/1.JATIS.3.4.049002.

C. Moriarty, K. Brooks, R. Soummer, M. Perrin, T. Comeau, G. Brady, R. Gontrum, and P. Petrone. High-contrast imager for complex aperture telescopes (HiCAT): 6. software control infrastructure and calibration. In *Space Telescopes and Instrumentation 2018: Optical, Infrared, and Millimeter Wave*, volume 10698 of *Society of Photo-Optical Instrumentation Engineers (SPIE) Conference Series*, page 1069853, August 2018. doi: 10.1117/12.2314058.

M. N'Diaye, E. Choquet, L. Pueyo, E. Elliot, M. D. Perrin, J. K. Wallace, T. Groff, A. Carlotti, D. Mawet, M. Sheckells, S. Shaklan, B. Macintosh, N. J. Kasdin, and R. Soummer. High-contrast imager for complex aperture telescopes (HiCAT): 1. testbed design. In *Techniques and Instrumentation for Detection of Exoplanets VI*, volume 8864 of *Proc. SPIE*, page 88641K, September 2013a. doi: 10.1117/12.2023718.

M. N'Diaye, K. Dohlen, T. Fusco, and B. Paul. Calibration of quasi-static aberrations in exoplanet direct-imaging instruments with a Zernike phase-mask sensor. *Astron. & Astrophys.*, 555:A94, July 2013b. doi: 10.1051/0004-6361/201219797.

M. N'Diaye, E. Choquet, S. Egron, L. Pueyo, L. Leboulleux, O. Levecq, M. D. Perrin, E. Elliot, J. K. Wallace, E. Hugot, M. Marcos, M. Ferrari, C. A. Long, R. Anderson, A. DiFelice, and R. Soummer. High-contrast Imager for Complex Aperture Telescopes (HICAT): II. Design overview and first light results. In *Society of Photo-Optical Instrumentation Engineers (SPIE) Conference Series*, volume 9143 of *Society of Photo-Optical Instrumentation Engineers (SPIE) Conference Series*, page 27, August 2014a. doi: 10.1117/12.2056694.

M. N'Diaye, K. Dohlen, A. Caillat, A. Costille, T. Fusco, A. Jolivet, F. Madec, L. Mugnier, B. Paul, J.-F. Sauvage, R. Soummer, A. Vigan, and J. K. Wallace. Design optimization and lab demonstration of ZELDA: a Zernike sensor for near-coronagraph quasi-static measurements. In *Society of Photo-Optical Instrumentation Engineers (SPIE)*

Conference Series, volume 9148 of *Society of Photo-Optical Instrumentation Engineers (SPIE) Conference Series*, page 5, August 2014b. doi: 10.1117/12.2056818.

M. N'Diaye, J. Mazoyer, É. Choquet, L. Pueyo, M. D. Perrin, S. Egron, L. Leboulleux, O. Levecq, A. Carlotti, C. A. Long, R. Lajoie, and R. Soummer. High-contrast imager for complex aperture telescopes (HiCAT): 3. first lab results with wavefront control. In *Techniques and Instrumentation for Detection of Exoplanets VII*, volume 9605 of *Proc. SPIE*, page 96050I, September 2015. doi: 10.1117/12.2188497.

B. Paul, J. F. Sauvage, and L. M. Mugnier. Coronagraphic phase diversity: performance study and laboratory demonstration. *Astron. & Astrophys.*, 552:A48, Apr 2013. doi: 10.1051/0004-6361/201220940.

M. Perrin, J. Long, E. Douglas, A. Sivaramakrishnan, and C. Slocum. POPPY: Physical Optics Propagation in PYthon. Astrophysics Source Code Library, February 2016.

I. Poberezhskiy, F. Zhao, X. An, K. Balasubramanian, R. Belikov, E. Cady, R. Demers, R. Diaz, Q. Gong, B. Gordon, R. Goullioud, F. Greer, O. Guyon, M. Hoenk, N. J. Kasdin, B. Kern, J. Krist, A. Kuhnert, M. McElwain, B. Mennesson, D. Moody, R. Muller, B. Nemati, K. Patterson, A. J. Riggs, D. Ryan, B.-J. Seo, S. Shaklan, E. Sidick, F. Shi, N. Siegler, R. Soummer, H. Tang, J. Trauger, J. K. Wallace, X. Wang, V. White, D. Wilson, K. Yee, H. Zhou, and N. Zimmerman. Technology development towards WFIRST-AFTA coronagraph. In *Society of Photo-Optical Instrumentation Engineers (SPIE) Conference Series*, volume 9143 of *Society of Photo-Optical Instrumentation Engineers (SPIE) Conference Series*, page 0, August 2014. doi: 10.1117/12.2060320.

L. Pogorelyuk and N. J. Kasdin. Dark Hole Maintenance and A Posteriori Intensity Estimation in the Presence of Speckle Drift in a High-Contrast Space Coronagraph. *arXiv e-prints*, February 2019.

L. Pueyo. Detection and Characterization of Exoplanets using Projections on Karhunen Loeve Eigenimages: Forward Modeling. *Astrophysical Journal*, 824:117, June 2016. doi: 10.3847/0004-637X/824/2/117.

L. Pueyo, J. Kay, N. J. Kasdin, T. Groff, M. McElwain, A. Give'on, and R. Belikov. Optimal dark hole generation via two deformable mirrors with stroke minimization. *Applied Optics*, 48:6296, November 2009. doi: 10.1364/AO.48.006296.

L. Pueyo, R. Soummer, J. S. Knight, and l. coyle. Stability error budget for exo-earth imaging with a large segmented telescope in space. In *American Astronomical Society Meeting Abstracts #233*, volume 233 of *American Astronomical Society Meeting Abstracts*, page 158.24, January 2019.

A. J. E. Riggs, N. J. Kasdin, and T. D. Groff. Recursive starlight and bias estimation for high-contrast imaging with an extended Kalman filter. *Journal of Astronomical Telescopes, Instruments, and Systems*, 2(1):011017, January 2016. doi: 10.1117/1.JATIS.2.1.011017.

B.-J. Seo, B. Gordon, B. Kern, A. Kuhnert, D. Moody, R. Muller, I. Poberezhskiy, J. Trauger, and D. Wilson. Hybrid Lyot coronagraph for wide-field infrared survey telescope-astrophysics focused telescope assets: occulter fabrication and high contrast narrowband testbed demonstration. *Journal of Astronomical Telescopes, Instruments, and Systems*, 2(1):011019, January 2016. doi: 10.1117/1.JATIS.2.1.011019.

B.-J. Seo, E. Cady, B. Gordon, B. Kern, R. Lam, D. Marx, D. Moody, R. Muller, K. Patterson, I. Poberezhskiy, C. Mejia Prada, E. Sidick, F. Shi, J. Trauger, and D. Wilson. Hybrid Lyot coronagraph for WFIRST: high-contrast broadband testbed demonstration. In *Society of Photo-Optical Instrumentation Engineers (SPIE) Conference Series*, volume 10400 of *Society of Photo-Optical Instrumentation Engineers (SPIE) Conference Series*, page 104000F, September 2017. doi: 10.1117/12.2274687.

G. Serabyn. Demonstrations of Deep Starlight Rejection with a Vortex Coronagraph , https://exoplanets.nasa.gov/exep/technology/TDEM-awards/. *TDEM white paper*, 2010.

G. Serabyn. Broadband Light Rejection with the Optical Vortex Coronagraph, https://exoplanets.nasa.gov/exep/technology/TDEM-awards/. *TDEM white paper*, 2014.

F. Shi, E. Cady, B.-J. Seo, X. An, K. Balasubramanian, B. Kern, R. Lam, D. Marx, D. Moody, C. Mejia Prada, K. Patterson, I. Poberezhskiy, J. Shields, E. Sidick, H. Tang, J. Trauger, T. Truong, V. White, D. Wilson, and H. Zhou. Dynamic testbed demonstration of WFIRST coronagraph low order wavefront sensing and control (LOWFS/C). In *Society of Photo-Optical Instrumentation Engineers (SPIE) Conference Series*, volume 10400 of *Society of Photo-Optical Instrumentation Engineers (SPIE) Conference Series*, page 104000D, September 2017. doi: 10.1117/12.2274887.

R. Soummer, L. Pueyo, and J. Larkin. Detection and Characterization of Exoplanets and Disks Using Projections on Karhunen-Loève Eigenimages. *Astrophysical Journal, Letters*, 755:L28, August 2012. doi: 10.1088/2041-8205/755/2/L28.

R. Soummer, G. R. Brady, K. Brooks, T. Comeau, É. Choquet, T. Dillon, S. Egron, R. Gontrum, J. Hagopian, I. Laginja, L. Leboulleux, M. D. Perrin, P. Petrone, L. Pueyo, J. Mazoyer, M. N'Diaye, A. J. E. Riggs, R. Shiri,

A. Sivaramakrishnan, K. St. Laurent, A.-M. Valenzuela, and N. T. Zimmerman. High-contrast imager for complex aperture telescopes (HiCAT): 5. first results with segmented-aperture coronagraph and wavefront control. In *Space Telescopes and Instrumentation 2018: Optical, Infrared, and Millimeter Wave*, volume 10698 of *Society of Photo-Optical Instrumentation Engineers (SPIE) Conference Series*, page 106981O, August 2018. doi: 10.1117/12.2314110.

K. St. Laurent, K. Fogarty, N. T. Zimmerman, M. N'Diaye, C. C. Stark, J. Mazoyer, A. Sivaramakrishnan, L. Pueyo, S. Shaklan, R. Vanderbei, and R. Soummer. Apodized pupil Lyot coronagraphs designs for future segmented space telescopes. In *Space Telescopes and Instrumentation 2018: Optical, Infrared, and Millimeter Wave*, volume 10698 of *Society of Photo-Optical Instrumentation Engineers (SPIE) Conference Series*, page 106982W, July 2018. doi: 10.1117/12.2313902.

C. C. Stark, A. Roberge, A. Mandell, and T. D. Robinson. Maximizing the ExoEarth Candidate Yield from a Future Direct Imaging Mission. *Astrophysical Journal*, 795:122, November 2014. doi: 10.1088/0004-637X/795/2/122.

C. C. Stark, A. Roberge, A. Mandell, M. Clampin, S. D. Domagal-Goldman, M. W. McElwain, and K. R. Stapelfeldt. Lower Limits on Aperture Size for an ExoEarth Detecting Coronagraphic Mission. *Astrophysical Journal*, 808: 149, August 2015. doi: 10.1088/0004-637X/808/2/149.

H. Sun, N. J. Kasdin, R. Vanderbei, A. J. E. Riggs, and T. Groff. Improved high-contrast wavefront controllers for exoplanet coronagraphic imaging systems. In *Society of Photo-Optical Instrumentation Engineers (SPIE) Conference Series*, volume 10400 of *Society of Photo-Optical Instrumentation Engineers (SPIE) Conference Series*, page 104000R, September 2017. doi: 10.1117/12.2274720.

The LUVOIR Team. The LUVOIR Mission Concept Study Interim Report. *arXiv e-prints*, art. arXiv:1809.09668, Sep 2018.

M. Ygouf, L. Pueyo, R. Soummer, M. D. Perrin, R. van der Marel, and B. Macintosh. Data processing and algorithm development for the WFIRST-AFTA coronagraph: reduction of noise free simulated images, analysis and spectrum extraction with reference star differential imaging. In *Techniques and Instrumentation for Detection of Exoplanets VII*, volume 9605 of *Proc. SPIE*, page 96050S, September 2015. doi: 10.1117/12.2188669.

M. Ygouf, N. T. Zimmerman, L. Pueyo, R. Soummer, M. D. Perrin, B. E. Mennesson, J. E. Krist, G. Vasisht, B. Nemati, and B. A. Macintosh. Data processing and algorithm development for the WFIRST coronagraph: comparison of RDI and ADI strategies and impact of spatial sampling on post-processing. In *Space Telescopes and Instrumentation 2016: Optical, Infrared, and Millimeter Wave*, volume 9904 of *Proc. SPIE*, page 99045M, July 2016. doi: 10.1117/12.2231581.